Journal of Nuclear Materials 378 (2008) 134–138

Contents lists available at ScienceDirect

Journal of Nuclear Materials

journal homepage: www.elsevier.com/locate/jnucmat

Microstructure characterization of oxidation of aluminized coating prepared by a combined process

H.B. Liu, J. Tao *, J. Xu, Z.F. Chen, X.J. Sun, Z. Xu

College of Material Science and Technology, Nanjing University of Aeronautics and Astronautics, 29 Yudao Street, Nanjing 210016, PR China

ARTICLE INFO

Article history:
Received 22 January 2008
Accepted 22 May 2008

PACS:
82.33.Xj
81.07.Bc
61.43.Er
61.80.Jh

ABSTRACT

Alumina layer is a good candidate for the tritium penetration barrier that is important in the control of tritium losses due to permeation through structural materials used in high-temperature gas-cooled reactors and in fusion reactors. This paper describes the microstructure of the oxide film of the tritium penetration barrier formed on 316L stainless steel, which was prepared by a combined process, namely, aluminizing and oxidizing treatments using a double glow plasma technology. Microstructure and phase structure of the coatings investigated were examined by scanning electronic microscope (SEM), X-ray diffraction analysis (XRD) and transmission electron microscopy (TEM), respectively. The chemical composition and the chemical states of Al, O elements in the oxidation film were identified by X-ray photoelectron spectroscopy (XPS). After aluminization, the typical microstructure of the coating mainly consisted of an outer high aluminum-containing intermetallic compound layer (Fe_2Al_5 and FeAl) and intermediate ferritic stainless steel (α Fe(Al))layer followed by the austenitic substrate. After the combined process, an oxide layer that consisted of Al_2O_3 and spinel $FeAl_2O_4$ had been successfully formed on the aluminizing coating surface, with an amorphous outmost surface and an underlying subsurface nanocrystalline structure.

1. Introduction

Considerable efforts have been made in the last few years in order to reduce the losses of tritium due to permeation through structural materials in fusion reactors for its safety and operational implications. The use of coatings as tritium permeation barriers (TPB) is one of the possible solutions to cut down the tritium loss. In Europe, the emphasis of the coating development program is on an alumina/Al–Fe coating on reduced activation martensitic (RAM) steels in the spell out WCLL concept. In Japan, much attention is paid on electrically insulating coatings for the self-cooled lithium/vanadium system, as well as the coatings for the spell out breeder systems. Meanwhile, in Russia and the United States the research effort is focused on the development of electrically insulating coatings for the lithium/vanadium system [1,2]. It is known that the growth of oxide layers or the application of surface coatings can be used to provide effective hydrogen and tritium permeation barriers [3,4]. Previous measurements have shown that Al_2O_3 is one of the most promising materials for use as permeation barriers [5,6]. Several methods, such as hot dipping, vacuum plasma spray, pack-cementation and chemical vapour deposition, etc., have been developed to produce such oxide scale systems on stainless steel. Previous measurements of aluminides deposited by a hot dipping process on DIN 1.4914 martensitic steel indicated a permeation reduction factor (PRF) of more than three orders of magnitude [7]. $A1_2O_3$ deposited by CVD on AISI 316L and an alumina layer deposited by VPS on MANET exhibited reductions in tritium permeation of one order of magnitude and three orders of magnitude, respectively [8]. However a major drawback of those processes is the presence of varying degrees of porosity, both isolated and interconnecting, in the multiple splats of the coating thickness [9,10]. These defects are favorable to the diffusion of hydrogen or tritium in tritium penetration barrier, because the long-range diffusion will be influenced by extended defect structures, such as dislocation networks, grain or phase boundaries, or the texture of the multi-phase system [11].

The double glow plasma surface alloying technique is a modern technology in the field of surface alloying [12,13]. By comparison with other advanced surface alloying technologies, for instance, ion implantation and laser alloying, the double glow technique is less expansive for many potential users. The technology employs a low temperature plasma produced by glow discharge. By using this technique, an alloying layer with special physical, chemical properties can be obtained on the surface of metallic materials. For example, the nickel-base alloy layer, stainless steel layer and high-speed steel layer have been formed on the surface of the treated metallic materials. The depth of the alloying layer could vary from several different microns to 500 μm, with alloying elements in a concentration of few percent to 90% or more. Mono-element

* Corresponding author. Tel.: +86 25 52112900; fax: +86 25 52112626.
E-mail address: taojie@nuaa.edu.cn (J. Tao).

0022-3115/$ - see front matter © 2008 Elsevier B.V. All rights reserved.
doi:10.1016/j.jnucmat.2008.05.012

alloying of Ni, Cr, Mo, W, Ta, Al, Ti, etc. [14] and multi-element alloying of Ni–Cr, W–Mo, W–Mo–Cr–V, etc., have been studied [15–17]. In the present work, a combined process that includes aluminizing and oxidizing treatments using a double glow plasma technology, was used to prepare an oxide layer which consisted of Al_2O_3 and spinel $FeAl_2O_4$. The microstructural characterization and chemical composition of oxide film were examined.

2. Experimental procedures

The surface alloying experiments were performed in a double-glow plasma surface-alloying device, in which a low-temperature plasma was produced by a glow discharge process in a vacuum sputtering chamber [18]. The sketch is shown in Fig. 1. There are three electrodes: the anode and two negatively charged members, the cathode and the source electrode. The source electrode is made up of the desired alloying elements. When the two power supplies are turned on, both cathode and source electrode are surrounded by glow discharge. One glow discharge heats the substrate to be alloyed while the second glow discharge strikes the source electrode materials for supplying desired alloying elements. The desired alloying elements travel toward the substrate and diffuse into the substrate materials surface forming an alloying layer.

In the experiment, source material was pure Al. Substrate material was 316L stainless steel with a size of 60 mm × 30 mm × 5 mm and the chemical composition of this steel is shown in Table 1. The specimens were machined, ground, polished, ultrasonically cleaned in acetone and dried in air. The depositions were performed in argon atmosphere with an impulse discharge. After processing the substrate was cooled inside the chamber in an argon atmosphere. During the process of aluminizing, the glow discharge sputtering conditions were: working pressure, 35 Pa; source electrode voltage with direct current, 850 V; workpiece electrode voltage with impulse current, 250 V; and the parallel distance between the source electrode and the substrate, 20 mm, treatment time, 2 h. In order to obtain an oxide layer, the aluminizing coating was oxidized in the mixed ambient of argon and oxygen for 1 h at a partial oxygen pressure of 1 Pa.

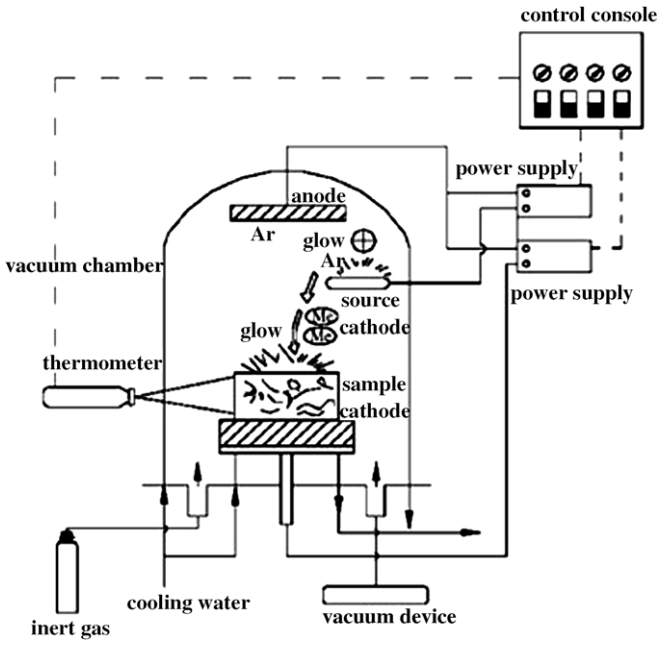

Fig. 1. Sketch of double-glow plasma surface alloying technology.

Table 1
Chemical composition of heat resistance stainless steel 316L in wt%

Si	C	Mn	P	S	Cr	Ni	Mo	N	Fe
0.229	0.027	1.716	0.032	0.001	16.936	10.128	2.215	0.046	Balance

The phases in the film were characterized by X-ray diffraction (XRD, Model D8ADVANCE) using monochromatic Cu Kα radiation. The cross-section of the metallographic specimen was abraded and polished, then cleaned with ethanol. Interface morphology was observed by scanning electron microscopy (SEM, Quanta200, FEI Company). The chemical composition of the interface was identified by means of an energy dispersive X-ray (EDX) analyzer coupled to the SEM instrument and by both an X-ray photoelectron spectroscopy (XPS, Model AXISULTRA, UK). The XPS spectra were recorded with monochromatized Al radiation (1486.71 eV) as the excitation source, at a constant power of 225 W (15 kV, 15 mA). The kinetic energies of photoelectrons were measured using a hemispherical electrostatic analyzer working in a constant pass energy mode. The C 1s peak from the adventitious carbon-based contaminant with binding energy of 284.8 eV was used as the reference for calibration. Detail microstructure of the film was examined using transmission electron microscopy (TEM, Model Tecnai $G^2$20, FEI Company). Thin slices, about 0.3 mm thick, were first cut from parallel section to the coating surface by wire-cut machine, and thinned by mechanical grinding and dimpling, then ion thinned by ion-beam milling technique until perforation.

3. Results and discussion

Plotted in Fig. 2(a) is a typical X-ray diffraction patterns for the aluminizing sample. The characteristic peaks of FeAl and Fe_2Al_5 were seen. Although the substrate was austenitic stainless steel, its characteristic peaks were absent, indicating that a rather thick aluminized layer was formed on 316L stainless steel. According to the Fe–Al phase diagram [19], Fe_3Al, Fe_2Al_5, $FeAl_2$ and FeAl are present in close succession, but only Fe_2Al_5 and FeAl phases were observed in our experiment. The appearance of Fe_2Al_5 phase was due to the preferential formation for its low atom concentration along the *C*-axis [20]. In addition, the activation energy of FeAl growth (180 kJ/mol) was lower than that of Fe_3Al (260 kJ/mol) [21]. Therefore, the growth of Fe_3Al might be slower than that of the FeAl phase. After oxidation of aluminizing coating, the coating mainly consisted of the spinel phase $FeAl_2O_4$, the FeAl and Fe_2Al_5 phases, seeing Fig. 2(b). Comparing to Fig. 2(a), it is obviously seeing that the peak intensities of the Fe_2Al_5 phase decreased which was attributed to a part of Fe–Al intermetallic compound had been transformed into oxide. The spinel $FeAl_2O_4$ phase had been reported previously in the oxidation of iron–aluminum alloys by Prescott [22]. It had been suggested that $A1_2O_3$ might then react with Fe_2O_3 to form nodules of the phase $Fe_2O_3 \cdot Al_2O_3$ (or $FeA1O_3$) and this unstable $Fe_2O_3 \cdot Al_2O_3$ phase might transform to $FeA1_2O_4$ which had a greater effect at blocking the diffusion of Fe. In Ref. [23]. It was reported that the presence of $FeAl_2O_4$ depended on the Fe_2O_3:Al ratio, appearing firstly the oxygen available (i.e. the Fe_2O_3 amount) was above the stoichiometric amount, and secondly the aluminum was in excess.

Typical cross section microstructures of aluminizing coating are shown in Fig. 3(a). The aluminizing coating was continuous and compact without any visible metallurgy flaw. The coating thickness was about 30 μm and showed three different areas within the coating. The composition of various microzones by energy dispersive X-ray (EDX) was given in Table 2. Based on the combined the results of XRD and chemical composition of regions in coating, it indicated that the upper layer yielded a composition of 68.23 at.%

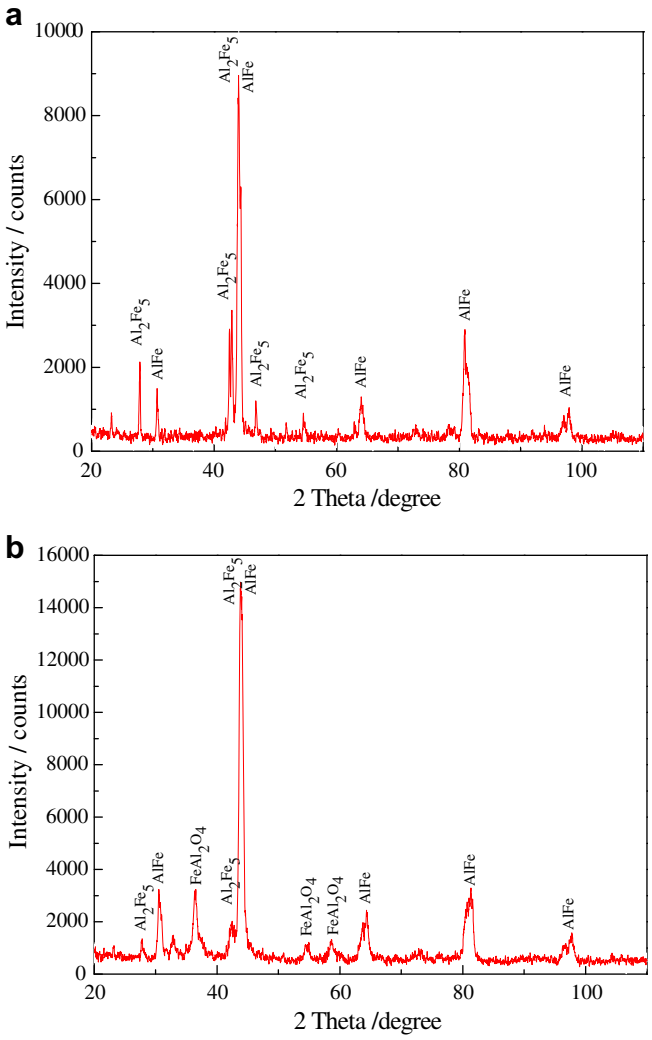

Fig. 2. X-ray diffraction patterns of (a) the aluminizing sample and (b) the oxide sample.

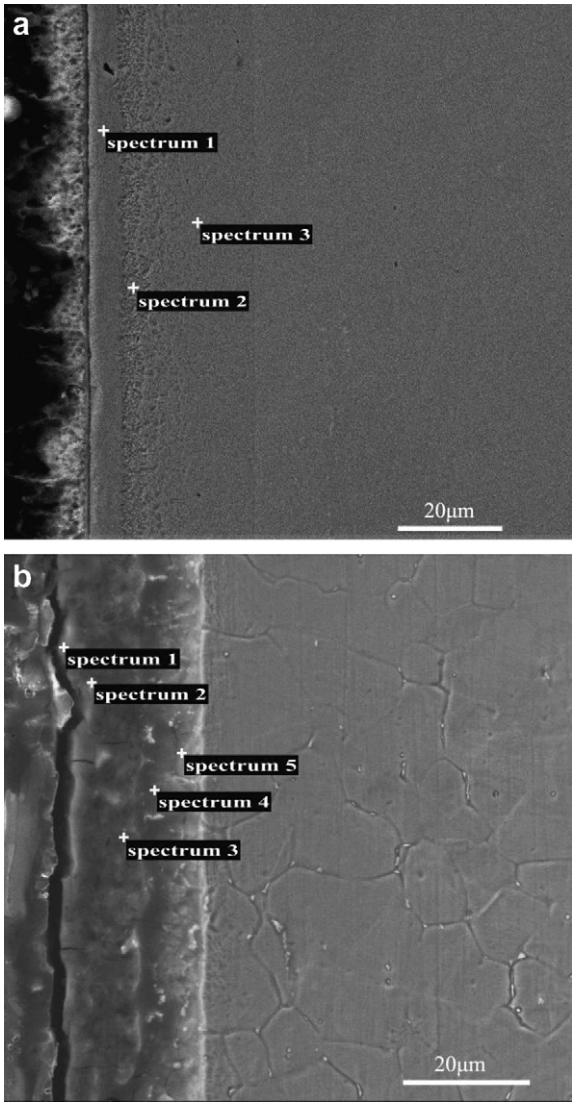

Fig. 3. Microstructure of (a) the aluminizing sample and (b) the oxide sample.

Al and 23.74 at.% Fe which corresponded to the Fe_2Al_5 phase; the middle layer showed 39.68 at.% Al and 37.63 at.% Fe, corresponding to the FeAl phase; while the inner layer displayed 12.03 at.% Al and 61.76 at.% Fe, which corresponded to the α-Fe(Al) phase. The existence of α Fe(Al) phase was due to the fact that Al is a ferrite stabilizer, the high Al content in the aluminide layer cause the transformation of austenite to ferrite with diffusion of Al into substrate. These results were consistent with the literature [24,25].

The cross-sectional micrograph of oxidized specimen is depicted in Fig. 3(b) with its corresponding EDX spot analysis shown in Table 3. The thickness of the intermetallic layer after oxidation was reduced due to the diffusion of aluminum into steel base. Four distinct layers were observed. According to the composition analysis, the whole layer was able to be divided into four different microzones. A continuous alumina-rich oxide film was formed at the outermost surface of the specimen, corresponding to spectrum '1' and '2' in Fig. 3(b). At the outermost the white phase (marked spectrum '1') with the atomic ratio of O to A1 was 63.35 to 24.02 which corresponded to the alumina. Owing to thin thickness of alumina, the peak of Al_2O_3 had not been found by the X-ray diffraction spectra. The inner oxide layer (spectrum '2') with the content of O, Al and Fe was 55.82 at.%, 21.82 at.% and 14.49 at.% indicated the possibility of a $FeAl_2O_4$ spinel phase detected by XRD. Besides, the coating after oxidation still consisted of Fe_2Al_5 phase and FeAl compounds (refer to the analysis results (Table 3) of spectrum '3' and '4' in Fig. 3(b)) and Al diffused layer were formed at the

Table 2
EDS results of the spectrums of Fig. 3(a) in at.%

Element	Spectrum1	Spectrum2	Spectrum3
Al	68.23	39.68	12.03
Fe	23.74	37.63	61.76
Cr	05.43	07.75	19.33
Ni	01.64	14.24	05.06
Mo	00.96	00.71	01.82

Table 3
EDS results of the spectrums of Fig. 3(b) in at.%

Element	Spectrum1	Spectrum2	Spectrum3	Spectrum4	Spectrum5
O	63.35	55.82	–	–	–
Al	24.02	21.82	84.55	49.15	15.73
Fe	08.20	14.49	12.35	39.14	59.27
Cr	02.26	05.57	02.57	06.78	17.40
Ni	01.20	01.64	00.82	03.46	06.04
Mo	00.97	00.66	00.26	01.48	01.56

position of spectrum '5'. Accordingly, after the combined process, it resulted in the formation of a top oxide layer on intermetallic layer and the structure of such coating was mainly SS/α-Fe(Al)/FeAl/Fe_2Al_5/$FeAl_2O_4$/Al_2O_3.

In order to investigate the chemical composition of the oxide film at different thickness, depth profiling on the surface alloying layer versus sputter time is shown in Fig. 4. It showed that O content decreased with the increase of sputter time, falling to 40.11 from 64.02 at.% after sputtering for 10 min. Meanwhile, Al content continuously increased with the sputtering time. Fig. 5 presents the XPS spectra of Al 2p and O 1s for the oxide sample after sputtering different time, respectively. The Al2p spectra shown in Fig. 5(a) contained one single component with a binding energy of around 74.53 eV. This binding energy was typical of aluminium in its oxidized form (Al_2O_3) [26]. The O 1s photoelectron spectra obtained was in good agreement with the aforementioned Al 2p spectra shown in Fig. 5(b). Based on XPS measurements shown above, it could be concluded that the oxide sample was enriched in Al_2O_3. An oxide layer formed on the surface of the sputtered coating and acted as a barrier layer, separating the substrate surface from the aggressive deposits [27]. With increasing time, there was not enough Al to maintain pure Al_2O_3. Then the O^{2-} permeated into the coating and reacted mainly with Fe to form Fe_3O_4 or Fe_2O_3, which possibly reacted with Al_2O_3 to get the spinels phase $FeAl_2O_4$ [28].

High resolution TEM (HRTEM) observation found an amorphous layer on the outermost surface and an underlying nanocrystalline layer with a grain size of <10 nm (seeing Fig. 6). The upper right-hand corner of Fig. 6 is a selected area electron diffraction pattern (SAED) of the surface amorphous region. The halo ring pattern of amorphous region and high-resolution image (the bottom right-hand corner of Fig. 6) confirmed that the outermost surface layer of the oxide film was completely amorphous.

Previous research on the oxidation of low-index FeA1 surfaces at temperatures up to 500 °C under UHV conditions led to the formation of amorphous Al_2O_3 films with approximately 0.5 nm thickness [29]. In this work, the Al_2O_3 obtained exhibited exceptional structure of the outmost surface amorphous layer and the underlying subsurface of nanocrystalline layer at a higher oxide temperature of 600 °C. Various occurrences of these radiation-induced amorphous or nanostructured products in the solid state had been reported [30–32]. In the irradiation technique, various defects were induced in the films due to the considerable irradiation energy and ultimately an amorphous state was obtained. In the double-cathode mode [33,34], both target cathode and substrate cathodes were subject to argon ion sputter by glow discharge. As a result, a large number of nanoparticles, which escaped from the surface of one cathode material and subsequently deposited on the surface of the other cathode materials surface, could transform into an amorphous structure. However, the crystallization of the deposited nanosized particles was inevitable as a result of inhomogeneous nucleation by substrate materials. Therefore, the underlying subsurface layer of the film became nanocrystalline.

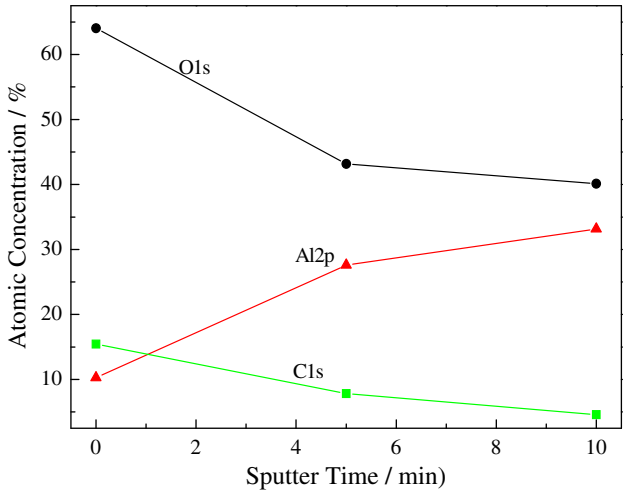

Fig. 4. Depth composition profile of the oxide film.

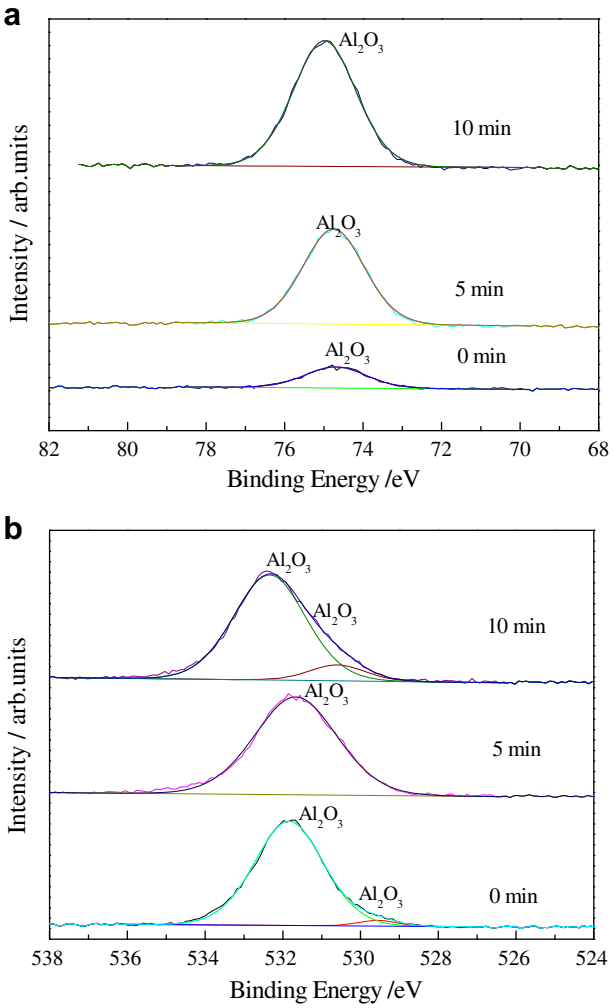

Fig. 5. XPS spectrum of the Al2p and O1s peak of the oxide sample.

According to the work of Wenhai Song [35], the permeability of the Al alloy treated by various oxidation processes decreased by nearly one order of magnitude, which suggests that aluminum oxide/hydroxide, whether crystalline or amorphous, had an appreciable hydrogen permeation resistance effect. In the case of the hydrogen diffusion in nanocrystalline alloys [11], this structure was reported to be similar to an amorphous state. Therefore, it can be speculated that the amorphous/nanocrystal Al_2O_3 coating is effective as a tritium penetration barrier. Further work should be done to find intrinsic relation between the magnitude of hydrogen permeability and phase components of the oxide layers formed.

4. Conclusions

In this work, an aluminium and alumina coating on 316L stainless were fabricated by means of the double glow plasma

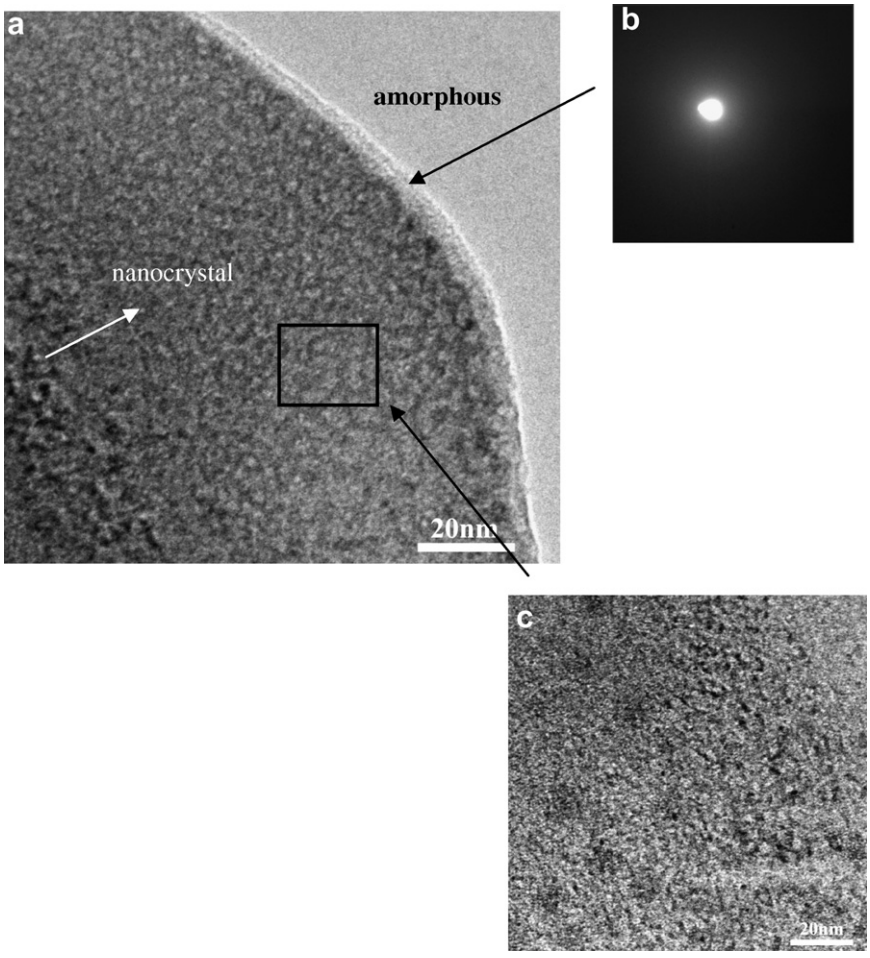

Fig. 6. TEM image of the oxide film. (a) The image shows that the film was composed of surface amorphous and subsurface nanocrystal. (b) The high-resolution image of amorphous area and the SAED pattern of the amorphous film. (c) A TEM image of subsurface nanocrystal film.

technique. The aluminizing coating was composed of three layers with Fe_2Al_5, FeAl and α Fe(Al). After the sputtering deposition of Al, oxidation was performed in argon and oxygen atmosphere. A continuous Al_2O_3 film was formed at the outermost surface, followed by the spinel $FeAl_2O_4$. In the meantime, the coating after oxidation still consisted of Fe_2Al_5, FeAl compounds and α Fe(Al) phase. It was found that a large area amorphous/nanocrystal Al_2O_3 films was able to be prepared by this technique. The film exhibited exceptional structure that the outmost surface of the films was amorphous and the underlying subsurface was nanocrystal with a grain size of <10 nm.

Acknowledgment

The authors gratefully acknowledge financial support from the National Natural Science Foundation of China (50571045).

References

[1] D.L. Smith, J. Konys, T. Muroga, V. Evitkhin, J. Nucl. Mater. 307–311 (2002) 1314.
[2] A. Perujo, H. Kolbe, J. Nucl. Mater. 258–263 (1998) 582.
[3] E. Serra, P.J. Kelly, D.K. Ross, R.D. Arnell, J. Nucl. Mater. 257 (1998) 194.
[4] K.S. Forcey, D.K. Ross, C.H. Wu, J. Nucl. Mater. 182 (1991) 36.
[5] R. Conrad, K. Bakker, C. Chabrol, M.A. Fütterer, J.G. van der Laan, E. Rigal, M.P. Stijkel, J. Nucl. Mater. 283–287 (2000) 1351.
[6] A. Aiello, A. Ciampichetti, G. Benamati, J. Nucl. Mater. 329–333 (2004) 1398.
[7] E. Serra, H. Glasbrenner, A. Perujo, Fusion Eng. Design 41 (1998) 149.
[8] A. Perujo, K.S. Forcey, Fusion Eng. Design 28 (1995) 252.
[9] H. Glasbrenner, J. Konys, Z. Voss, O. Wedemeyer, J. Nucl. Mater. 307–311 (2002) 1360.
[10] G. Benamati, C. Chabrol, A. Perujo, E. Rigal, H. Glasbrenner, J. Nucl. Mater. 271–272 (1999) 391.
[11] M. Hirscher, J. Mössinger, H. Kronmüller, J. Alloys Compd. 231 (1995) 267.
[12] Z. Xu, US Patent, No. 4520268, 1985.
[13] Z. Xu, US Patent, No. 4, 520, 268; US Patent, 4, 731, 539; UK Patent, No. 2, 150, 602; Canada Patent, No. 1, 212, 486; Australia Patent No. 580, 734; Sweden Patent, No. 8, 500, 364-8; Japanese Patent 1, 872, 305.
[14] Z. Xu, Z. Wang, F. Gu, Trans. Metal Heat Treat. 1 (1982) 71. in Chinese.
[15] J. Xu, X.S. Xie, Z. Xu, Trans. Metal Heat Treat. 1 (2002) 28. in Chinese.
[16] Z. Xu, R. Liu, Z. Xu, Adv. Mater. Process. 12 (1997) 33.
[17] B. Fan, Z. Xu, Heat Treat. Metal 9 (1988) 42. in Chinese.
[18] Jiang Xu, Zhang Xu, Xie Xishan, Xu Zhong, Liu Wenjin, Vacuum 72 (2004) 489.
[19] Koji Murakami, Norihide Nishida, Kozo Osamura, Yo Tomota, Acta Mater. 52 (2004) 1271.
[20] Deqing Wang, Ziyuan Shi, Appl. Surf. Sci. 227 (2004) 255.
[21] T.L. Hu, H.L. Huang, D. Gan, T.Y. Lee, Surf. Coat. Technol. 201 (2006) 3502.
[22] R. Prescott, M.J. Graham, Oxi. Metal 38 (1992) 73–87.
[23] Luísa Durães, Benilde F.O. Costa, Regina Santos, António Correia, José Campos, António Portugal, Mater. Sci. Eng. A 465 (2007) 199.
[24] Tomohiro Sasaki, Takao Yakou, Surf. Coat. Technol. 201 (2006) 2131–2139.
[25] L. Dumitrescu, F. Maury, Surf. Coat. Technol. 125 (2000) 419.
[26] S. Rana, S. Ram, S. Seal, S.K. Roy, Appl. Surf. Sci. 236 (2004) 141.
[27] Xin Ren, Fuhui Wang, Surf. Coat. Technol. 201 (2006) 30.
[28] A. Bataille, A. Addad, J. Crampon, R. Duclos, J. Eur. Ceram. Soc. 25 (2005) 857.
[29] H. Graupner, L. Hammer, K. Heinz, D.M. Zehner, Surf. Sci. 380 (1997) 335.
[30] S. Utsunomiya, L.M. Wang, S. Yudintsev, R.C. EwingJ. Nucl. Mater. 303 (2002) 177.
[31] L.M. Wang, S.X. Wang, R.C. Ewing, A. Meldrum, R.C. Birtcher, Mater. Sci. Eng. A 286 (2000) 72.
[32] J. Lian, S.X. Wang, L.M. Wang, R.C. Ewing, J. Nucl. Mater. 297 (2001) 89.
[33] Jiang Xu, Jie Tao, Zheyuan Chen, Wenhui Zhu, Shuyun Jiang, Zhong Xu, Surf. Coat. Technol. 202 (2007) 577.
[34] Jiang Xu, Zhong Xu, Jie Tao, Zili Liu, Zheyuan Chen, Wenhui Zhu, Scripta Mater. 57 (2007) 587.
[35] Wenhai Song, Jiaju Du, Yongli Xu, Bin Long, J. Nucl. Mater. 246 (1997) 139.